LARGE-EDDY SIMULATION OF THERMALLY INDUCED OSCILLATIONS IN THE CONVECTIVE BOUNDARY LAYER

Marcus Oliver LETZEL[1] and Siegfried RAASCH[2]

[1]Member of JSCE, MSc, Dept. of Civil Engineering, Tokyo Institute of Technology (2-12-1 Ookayama, Meguro-ku, Tokyo 152-8852, Japan)

[2]Dr. rer. nat., Inst. of Meteorology and Climatology, University of Hannover (Herrenhäuser Str. 2, 30419 Hannover, Germany)

Mesoscale circulations induced by differential boundary layer heating due to surface inhomogeneities on scales of 5 km and more can significantly change the average properties and the structure of the convective boundary layer (CBL) as well as trigger off temporal oscillations. The results of one of the first numerical case studies using Large-Eddy Simulation (LES) on the mesoscale suggest that mesoscale circulations exhibit a considerably larger average kinetic energy than convection under homogeneous conditions.

This case study uses the Hannover LES model PALM with prescribed 1D sinusoidal surface heat flux variations on wavelengths from 2.5 to 40 km. The resulting mesoscale circulations are analyzed by means of domain-averaged cross-sections, time averaged and normalized with the boundary layer height, as well as domain-averaged time series.

The simulated mesoscale circulations were periodic. Vertical profiles and time series demonstrate that the onset of the mesoscale circulation triggers off a temporal boundary layer oscillation, whose period and amplitude depend on the surface heat flux perturbation wavelength and amplitude and on the background wind component perpendicular to the surface inhomogeneity orientation. A hypothesis of the oscillation mechanism is briefly discussed.

Key Words: *mesoscale circulation, oscillation, thermal surface inhomogeneity, convective boundary layer, Large-Eddy Simulation*

1. INTRODUCTION

Inhomogeneity on a wide range of spatial and temporal scales is a key feature of the Earth's surface. Variability in, for example, terrain, vegetation, soil texture and wetness, cloud cover and land-use leaves its first imprints on the atmosphere in the atmospheric boundary layer (ABL). The sudden or gradual changes in radiative, thermal, moisture and aerodynamic surface properties such as surface heat, momentum and humidity fluxes, surface roughness, temperature, wetness, and elevation affect the ABL flow structure and associated atmospheric processes, e.g. alter convection or precipitation.

The heterogeneous surface information usually translates into the ABL dynamically[1)] or thermally[2)]. Both have been subject of active research over the past two decades. Recent numerical case studies[3)4)5)] point at heterogeneous surface heat fluxes playing a key role here. Via differential ABL heating they produce horizontal pressure gradients that initiate the mesoscale circulation. The effect of such a thermally induced mesoscale circulation (TMC) can extend well into the free atmosphere up to the mid-troposphere[6)].

This numerical study reveals for the first time that in many cases the TMC onset induces a temporal oscillation of ABL flow, which significantly changes both average statistical properties and mean profiles. It identifies the parameters on which the oscillation depends and provides a hypothesis of the oscillation mechanism.

In order to bring out the new oscillation phenomenon clearly, this study idealizes surface heat flux heterogeneity as simple sine waves. Simulations of complex heterogeneous conditions are in preparation.

2. NUMERICAL EXPERIMENT

(1) Model Description

The *PA*rallel *L*arge-Eddy Simulation *M*odel (PALM) used for this study has been developed over the last years by the LES Group of the Institute of Meteorology and Climatology at the University of Hannover[7)8)]. Up-to-date model documentation is available at http://www.muk.uni-hannover.de/~raasch/PALM-1/intro_e.html.

In its dry mode used here PALM solves the Navier-Stokes equations in Boussinesq form, the 1st law of thermodynamics, and the equation for turbulent kinetic energy (TKE). Non-divergent flow is assured by solving a Poisson equation for the so-called pressure perturbation using Fast Fourier Transforms. Sub-gridscale (SGS) turbulence is parameterized according to the

suggestions of Deardorff [9] with minor alterations. This study uses PALM's standard finite differences method for the discretisation of the differential equations and the leap-frog scheme for the time integration. Lateral boundary conditions are cyclic, and Monin-Obukhov similarity is assumed in the Prandtl-layer between the surface and the first computational grid level.

(2) Experimental Setup

The starting point of this research was an open question of the study by Avissar and Schmidt[3] (hereafter AS98), hence the experimental design follows their case study to allow comparison.

2 h after simulation start, one-dimensional sinusoidal variations of amplitude A_x on wavelengths λ_x from 2.5 to 40 km were imposed on the near surface potential temperature flux $\overline{w'\theta'}$ (hereafter simply referred to as surface heat flux) so that

$$\overline{w'\theta'}(x) = \overline{w'\theta'}_{av} + A_x \sin\left(\frac{2\pi}{\lambda_x} x\right).$$

Large-scale atmospheric subsidence, typical of synoptic high-pressure conditions, was applied to the potential temperature profile only[10], but in contrast to AS98 a much weaker, more realistic[11] subsidence velocity of -2 cm s^{-1} was used. To compensate for the smearing effects of ABL growth, the xz cross-sections were additionally normalized by the ABL height z_i.

All simulations were run with a uniform grid spacing of 50 m, with a 9% vertical stretching above 1,800 m. The domain size was 5 km in y- and 3.2 km in z-direction, the width D_x is listed along with other simulation parameters for cases with zero background wind in **Table 1** and light wind in **Table 2**. D_x was generally chosen large enough to juxtapose at least two waves within the model domain, to allow eddy interaction. Calculations were carried out until at least two or three oscillation peaks were obtained. The cases denoted with a lower case "h" are corresponding homogeneous control runs. Cases A15 and B5 were run to reproduce the results of AS98 and are labeled accordingly.

The atmosphere was initialized with a weakly stable profile ($\partial\theta/\partial z$ = 0.8 K km^{-1}) up to a height of 1,200 m and a strong capping inversion above ($\partial\theta/\partial z$ = 7.4 K km^{-1}).

3. RESULTS

TMCs have already been well investigated and will therefore only be sketched here in brief. The main focus will be on the thermally induced oscillation.

Vertical profiles, xz cross-sections, and time series were used for ABL flow analysis.

(1) Thermally-Induced Mesoscale Circulation

Cases A15 and B5 reproduce very well the TMCs observed by AS98. For brevity, only one plot is provided to demonstrate this. **Fig. 1a** shows an xz cross-section of u for case A15 4h30 after simulation start, which is when the simulations of AS98 ended. (**Fig. 1b** shall be considered later.) The corresponding xz cross-section of w (not shown) exhibits a single strong updraft at x = 10 km, the maximum of the surface heat wave, only few weak adjacent updrafts at x = 0...20 km, and a large downdraft region at x = 20...40 km. u and w show a single dominant CBL circulation cell filling the entire domain, the TMC.

Table 1 Cases with zero background wind. (t_s: simulation time; other parameters defined in the text)

Case	D_x	λ_x	$\overline{w'\theta'}_{av}$	A_x	t_s
	km	km	K m s^{-1}	K m s^{-1}	h
A15	40	40	0.24	0.20	12
A15h	40	–	0.24	0	12
B5	40	40	0.12	0.10	12
B5h	40	–	0.12	0	12
L1	10	2.5	0.16	0.15	6
L1h	10	–	0.16	0	6
L2	10	5.0	0.16	0.15	6
L3	15	7.5	0.16	0.15	6
L4	20	10	0.16	0.15	9
L4A	20	10	0.16	0.10	9
L4B	20	10	0.16	0.05	9
L4C	20	10	0.16	0.03	9
L4D	20	10	0.16	0.01	9
L4h	20	–	0.16	0	11
L5	30	15	0.16	0.15	9
L6	40	20	0.16	0.15	9
L7	50	25	0.16	0.15	9
L7h	50	–	0.16	0	9
L8	30	30	0.16	0.15	11

Table 2 Cases with light background wind. (Base: reference case in Table 1; u_g, v_g: geostrophic wind along x and y)

Case	Base	u_g	v_g	t_s
		m s^{-1}	m s^{-1}	h
L4_u2	L4	2	0	6
L4_v2	L4	0	2	6
L4_u2h	L4h	2	0	6
L4_v2h	L4h	0	2	6
L8_u2	L8	2	0	11
L8_v2	L8	0	2	11
L8_u2h	L8h	2	0	11
L8_v2h	L8h	0	2	11

(2) Thermally-Induced Oscillation

a) Oscillation Existence

One of the main findings of this study is that the TMC intensity itself varies with time. AS98 already observed nonlinear vertical heat flux profiles at 4h30, which clearly points at non-quasi steady CBL development, but they could not observe oscillations because their simulations lasted only 4.5 h.

As soon as the heat wave is activated at 2 h, the

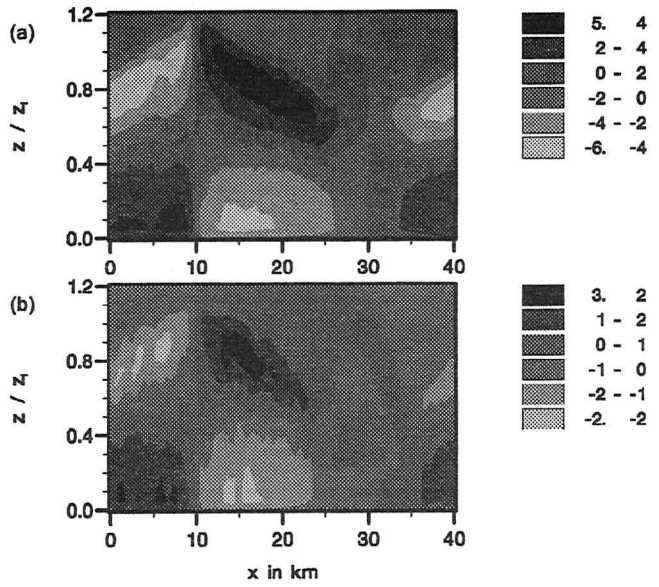

Fig. 1 xz cross-section of u in m s^{-1} for case A15 (a) 4h30 and (b) 6h15 after simulation start, z_i-normalized, averaged in y-direction and over the last 15 minutes.

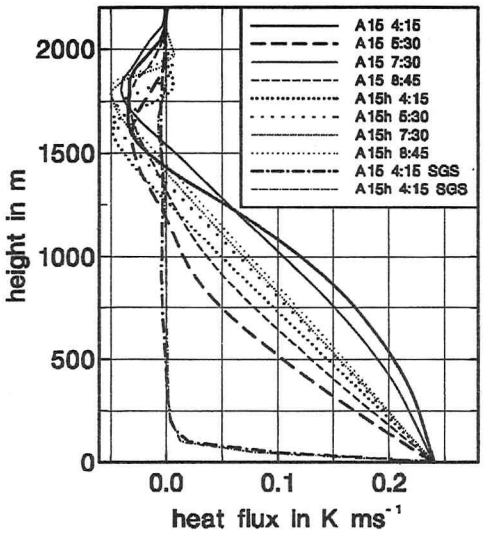

Fig. 2 Vertical heat flux profiles of cases A15 and A15h at selected times, averaged horizontally and over the last 15 minutes. The contribution of parameterized sub-gridscale (SGS) heat flux (dashed-dotted lines) is almost negligible.

linear vertical heat flux profile turns convex and reaches its maximum curvature at 4h15. Then it slowly changes to a near linear shape and turns concave with a maximum curvature at 5h30, returns to convex (7h30) and again concave shape (8h45). **Fig. 2** shows the profiles with extreme curvature together with the corresponding linear profiles of the homogeneous control run A15h.

In other words, the vertical heat flux divergence varies considerably throughout time. At times, the upper part of the CBL is heated more strongly than the lower one (convex shape), and vice versa (concave). And indeed, the vertical profiles of potential temperature (not shown) exhibit a sequence of stabilization followed by destabilization that corresponds well to the observed temporal variation of the heat flux profiles.

Strong evidence of the oscillation is provided by the time series of kinetic perturbation energy E* for cases A15 and B5 in **Fig. 3** that both describe a sine-like oscillation after the heat wave activation. The oscillation amplitude A_o decreases with time, presumably due to friction near the ground and in the entrainment layer (momentum exchange with non-moving air aloft). (**Fig. 2** shows that the maximum curvature, too, decreases with time.) Note that also the mean energy level itself increases dramatically compared with the homogeneous control runs.

Case B5 has not only a lower forcing heat flux mean and amplitude but also exhibits smaller A_o than A15. It requires more time to trigger off the oscillation, and it has a longer oscillation period T_o.

The maxima of the A15 time series coincide exactly with peak TMC strength (**Fig. 1a**), the minima with weakest TMC flow (**Fig. 1b**, halved intensity).

b) Oscillation Mechanism – a hypothesis

This subsection presents a hypothesis for the oscillation mechanism. The point is probably not so much the TMC onset itself (which can be attributed to horizontal surface heat flux, temperature and pressure gradients) – the key question seems to be what causes the TMC intensity to *decrease* (and *then* increase) again.

We suggest that it is the TMC itself that effectively reduces the horizontal temperature and pressure gradients that were responsible for its onset. Its forcing being reduced, the TMC itself should also decrease in strength. Meanwhile, the surface heat wave would of course continue to heat the lower part of the CBL inhomogeneously, thus acting to restore the TMC forcing. This would explain why the TMC intensity then again rises to a second peak.

The strength of the horizontal temperature, pressure and velocity gradients (not shown) indeed oscillates with time, which supports the hypothesis.

(3) Exploring the Parameter Space

In 3. (2) a) we already showed that the oscillation (A_o, T_o) varies with certain parameters. In this section we explore the parameter space and investigate how the oscillation depends on a) perturbation wavelength λ_x, b) amplitude A_x and c) background wind u_g and v_g.

a) Impact of Perturbation Wavelength λ_x

Fig. 4 shows time series of E* for cases that differ only in λ_x (and simulation time t_s). Their results differ in both oscillation period T_o and amplitude A_o. The larger λ_x, the larger T_o and A_o.

However, the smallest wavelengths, λ_x = 2.5 and 5 km (L1, L2), do not produce clear oscillations, and their average energy level even drops below that of the homogeneous control cases (L4h, L7h).

Fig. 4 further suggests that though the initially clear oscillations of cases L3 to L8 may cease after some time, their energy level will probably still remain much higher than in the homogeneous control cases.

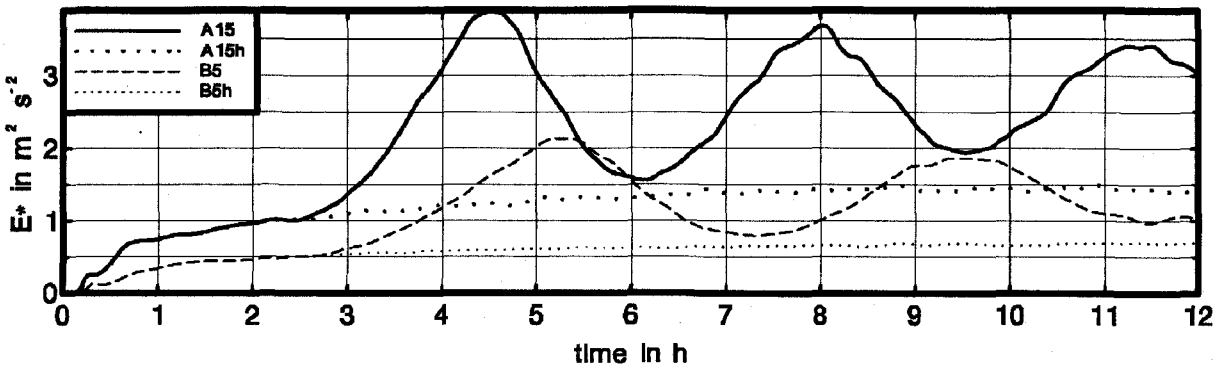

Fig. 3 Time series of kinetic perturbation energy E* for cases A15, B5 and their homogeneous control cases. Both A15 and B5 have 40 km wavelength, but A15 has double heat flux mean and amplitude.

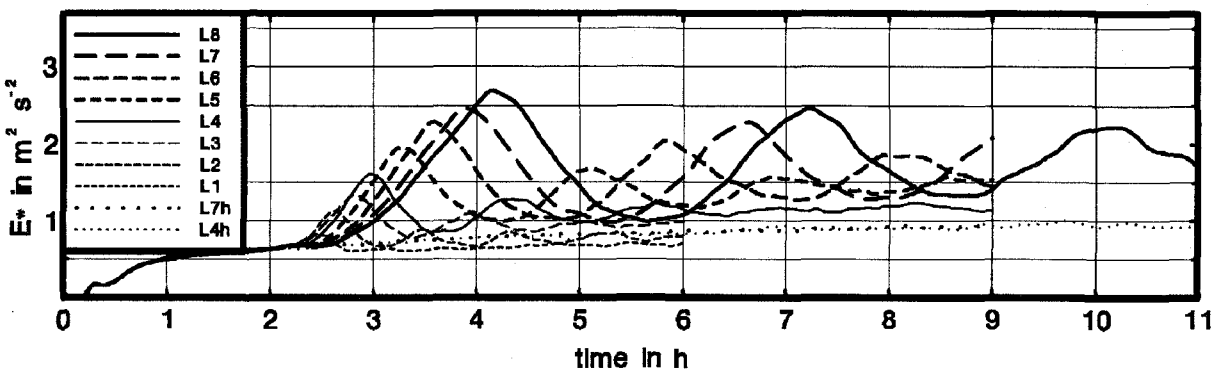

Fig. 4 Time series of kinetic perturbation energy E* for cases L1 to L8 with homogeneous control cases L4h and L7h. Cases L1 to L8 have same heat flux mean and amplitude but differ in wavelength and simulation time.

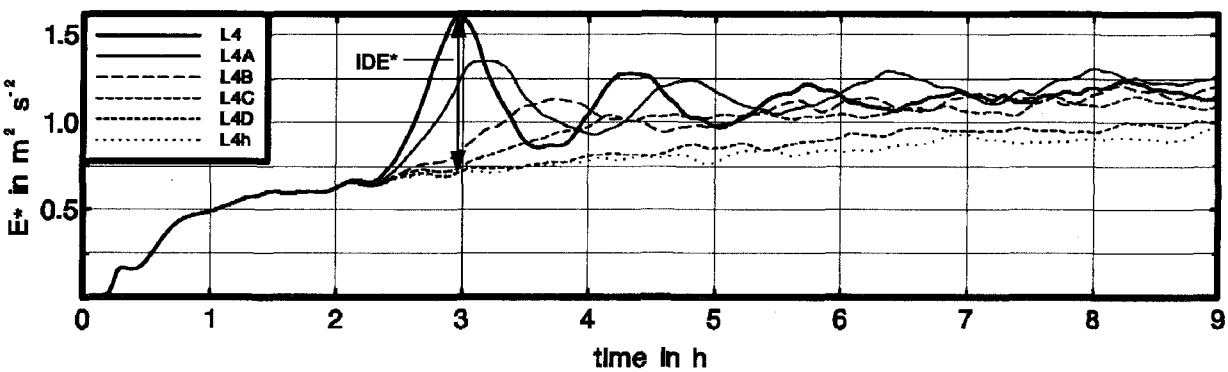

Fig. 5 Time series of kinetic perturbation energy E* for cases L4, L4A to L4D and their homogeneous control case L4h. These cases differ only in heat flux amplitude. (IDE* is an example how to derive the initial departure of kinetic energy E* from its corresponding homogeneous value for case L4; cf. subsection 3.3 (a).)

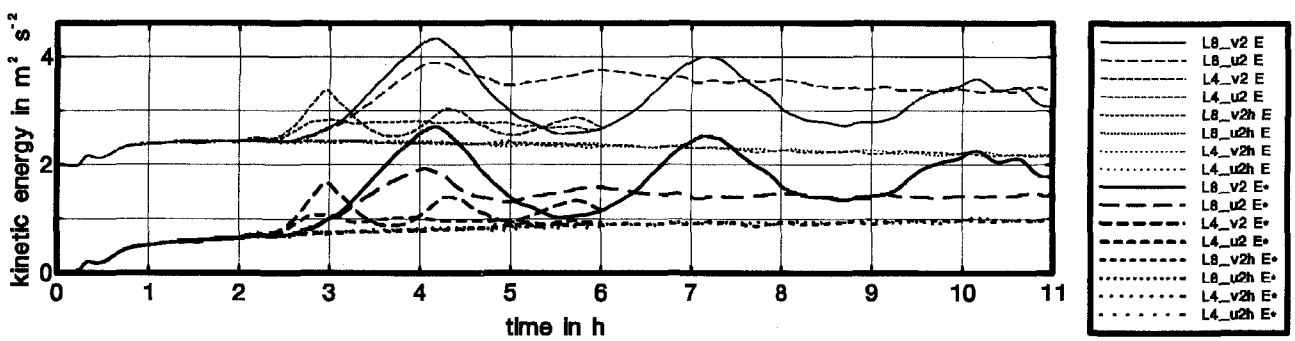

Fig. 6 Time series of total kinetic energy E and perturbation energy E* for all cases with background wind (**Table 2**) and their homogeneous control cases. These cases vary in wavelength, wind direction and simulation time.

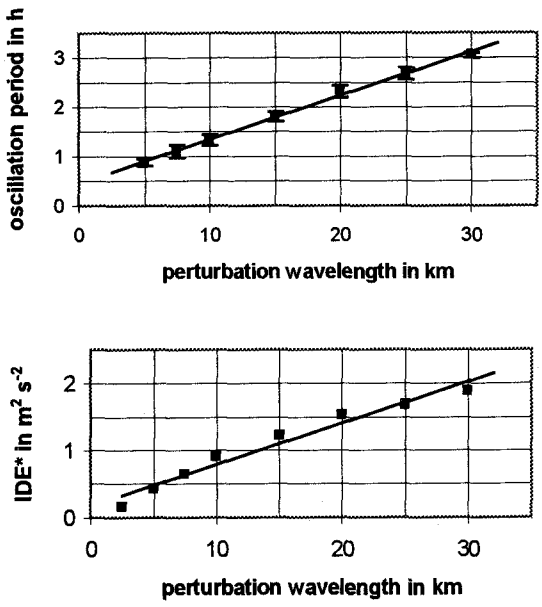

Fig. 7 Dependence of oscillation period T_o (top) and initial departure IDE* of kinetic energy E* from homogeneous control case (bottom) on the perturbation wavelength λ_x. Linear trend lines are added. Error bars (top) indicate the variability of T_o in the individual time series.

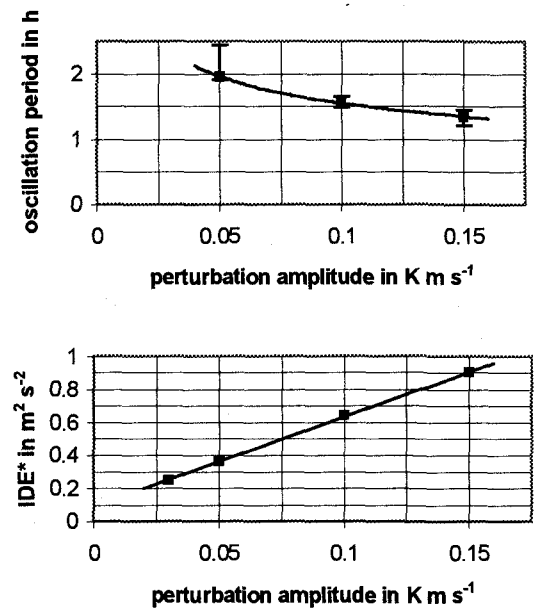

Fig. 8 Dependence of oscillation period T_o (top) and initial departure IDE* of kinetic energy E* from homogeneous control case (bottom) on the perturbation amplitude A_x. A power law and a linear trend line are added, respectively. For error bars cf. **Fig. 7**.

Fig. 7 (top) shows that T_o depends almost linearly on λ_x. As the oscillation amplitude A_o is difficult to measure a) because of its decrease with time and b) because of the slowly rising mean energy level, **Fig. 7** (bottom) instead depicts the initial departure IDE* of kinetic energy E* from its corresponding homogeneous value. (**Fig. 5** shows an example how to derive IDE*.) However, IDE* has no clear linear relationship with λ_x.

b) Impact of Perturbation Amplitude A_x

Fig. 5 shows time series of E* for cases that differ only in A_x. Their results also differ in both T_o and A_o. The larger A_x, the larger A_o but the smaller T_o.

However, the smallest amplitude, $A_x = 0.01$ K m s^{-1} (L4D), does not produce oscillations, and its average energy level is comparable to that of the homogeneous case L4h. I.e., there is a threshold of TMC formation between $A_x = 0.01$ and 0.03 K m s^{-1}.

Again, the energy level of those cases with clear oscillations (L4, L4A, L4B) remains considerably higher than in the homogeneous case (L4h).

Fig. 8 (top) indicates some nonlinear relationship between the oscillation period T_o and A_x. IDE* (bottom), however, shows a linear dependence on A_x.

The results of 3. (3) a) and b) suggest that the oscillation period T_o depends on the speed of the TMC onset. A large perturbation wavelength λ_x (weak horizontal surface heat flux gradient) or a small perturbation amplitude A_x (weak inhomogeneous heating) impede a quick TMC onset: the horizontal pressure gradients necessary for the TMC onset take longer to build up.

It is worth to note that the oscillation amplitude A_o increases not only with perturbation amplitude A_x (as one would expect), but also with perturbation wavelength λ_x. This is a nonlinear effect, because the TMC forcing, the horizontal gradient decrease with wavelength. The energy cascade may serve to explain this. At wavelengths near its peak at the natural scale of convection (2-3 km), the horizontal gradients due to the imposed inhomogeneities compete with those generated by the largest CBL eddies in natural convection and have to overcome their inertia to set up a TMC on this scale. At large wavelengths, however, this problem may not be so severe because on these scales the natural turbulence intensity has decreased by about an order of magnitude, making TMC generation easier.

c) Impact of Background Wind

Fig. 6 shows time series of kinetic energy for cases with weak background wind (2 m s^{-1}) that differ in both λ_x and wind direction. Because of the non-zero mean flow, total kinetic energy E and perturbation energy E* differ and are both plotted here.

In the cases with $u_g = 2$ m s^{-1} (L4_u2 and L8_u2; the wind blows across the surface inhomogeneity), enhanced turbulent shear in x-direction smears the surface information, weakens the TMC and rapidly dampens any initial TMC oscillations. Nevertheless E reaches significantly higher levels than in the corresponding control runs (L4_u2h and L8_u2h).

In the cases with $v_g = 2$ m s^{-1} (L4_v2 and L8_v2; the wind blows along the surface inhomogeneity), the background wind has almost no effect on the TMC and the oscillation: E* maxima and minima of cases L4_v2 and L8_v2 (**Fig. 6**) are synchronous with and equal in magnitude to those of the reference cases L4 and L8 (**Fig. 4**). Both E and E* of cases L4_v2 and L8_v2

reach significantly higher levels than in the corresponding control runs L4_v2h and L8_v2h (all **Fig. 6**).

Raasch and Harbusch[12] already noted that the background wind does not necessarily weaken TMCs. Only the component perpendicular to the orientation of the inhomogeneities does so. Even then, however, our study shows that the kinetic energy level remains much higher than in homogeneous simulations.

Souza et al.[13] presented a theory based on the second law of thermodynamics (the surface heat flux is proportional to the vertical temperature gradient at ground level) that well explains why surface inhomogeneities enhance the CBL circulation (hence increase the kinetic energy level). Under homogeneous conditions, the surface heat flux decreases when an air parcel advects towards an updraft because as it heats up, the difference between its own and the ground surface temperature decreases. However, in case of horizontal surface temperature gradients, the surface heat flux then decreases less rapidly. This allows higher horizontal temperature and pressure gradients.

This study directly prescribed the surface heat fluxes, which, following Souza et al.[13], leads to an even higher speed-up.

4. SUMMARY AND CONCLUSIONS

Oscillations have been identified which set in when TMCs on scales of 5 km and more develop. Their period and amplitude depend both on the scale and the intensity of the thermal surface forcing. With the TMC onset the kinetic energy level markedly increased and remained significantly higher than under homogeneous conditions.

These new findings might call into question those turbulence parameterizations employed by GCMs and other large-scale models that rely on homogeneous control runs of high-resolution models. Due to the periodic inhomogeneous forcing, its domain averaged value exactly equals that of a completely homogeneous model run – but the kinetic energy, for instance, on which many SGS parameterizations are based, deviates considerably.

The highly idealized character of this study and its predecessors[3) 4) 5)] calls for further research using more realistic surface conditions, for example diurnal heat flux variations, a superposition of inhomogeneities of different wavelength, amplitude, dimension and form, and the like. Higher wind speeds are worth to be addressed as well as the influence of latent heat flux.

Experimental proof is likely to be impeded by the high degree of complexity of natural landscapes and diurnal heat flux variations. Nevertheless, we would expect an atmospheric response on the scale of strongest surface inhomogeneity. TMC oscillations may occur e.g. over Antarctic coastal polynyas[14], where large ice-water patches might allow TMCs and oscillations even to persist over some days during the polar winter, or over continental lakes or patches of differently watered agricultural monocultures during summer. The upcoming EVA-GRIPS experiment in Germany is expected to give first answers to such questions.

ACKNOWLEDGEMENT: This research was supported by the Studienstiftung des deutschen Volkes in Bonn, Germany, and German BMBF Grants 07ATF37-UH and 01LD0103. Calculations were performed on the SGI/CRAY-T3Es of the Konrad-Zuse-Zentrum für Informationstechnik (ZIB) in Berlin, Germany, and the Regionales Rechenzentrum für Niedersachsen (RRZN) in Hannover, Germany. We wish to thank Manabu Kanda for his valuable comments and suggestions.

REFERENCES

1) Belcher, S.E. and Hunt, J.C.R.: Turbulent flow over hills and waves. *Ann. Rev. Fluid Mech.*, Vol.30, pp.507-538, 1998
2) Segal, M. and Arritt, R.W.: Nonclassical mesoscale circulations caused by surface sensible heat-flux gradients. *Bull. Amer. Meteor. Soc.*, Vol.73, pp.1593-1604, 1992
3) Avissar, R. and Schmidt, T.: An evaluation of the scale at which ground-surface heat flux patchiness affects the convective boundary layer using large-eddy simulation. *J. Atmos. Sci.*, Vol.55, pp.2666-2689, 1998
4) Gopalakrishnan, S.G. and Avissar, R.: An LES study of the impacts of land surface heterogeneity on dispersion in the convective boundary layer. *J. Atmos. Sci.*, Vol.57, pp.352-371, 2000
5) Baidya Roy, S. and Avissar, R.: Scales of response of the convective boundary layer to land-surface heterogeneity. *Geophys. Res. Lett.*, Vol.27, pp.533-536, 2000
6) Dalu, G.A., Pielke, R.A., Vidale, P.L. and Baldi, M.: Heat transport and weakening of atmospheric stability induced by mesoscale flows. *J. Geophys. Res.*, Vol.105, pp.9349-9363, 2000
7) Raasch, S. and Etling, D.: Modeling deep oceanic convection: large-eddy simulation in comparison with laboratory experiments. *J. Phys. Oceanogr.*, Vol.28, pp.1786-1802, 1998
8) Raasch, S. and Schröter, M.: PALM – A large-eddy simulation model performing on massively parallel computers. *Meteorol. Z.*, Vol.10, pp.363-372, 2001
9) Deardorff, J.W: Stratocumulus-topped mixed layers derived from a three-dimensional model. *Bound.-Layer Meteorol.*, Vol.18, pp.495-527, 1980
10) Khairoutdinov, M.F. and Kogan, Y.L.: A large eddy simulation model with explicit microphysics: Valication against aircraft observations of a stratocumulus-topped boundary layer. *J. Atmos. Sci.*, Vol.56, pp.2115-2131, 1999
11) Muschinski, A., Chilson, P.B., Kern, S., Nielinger, J., Schmidt, G. and Prenosil, T.: First frequency-domain interferometry observations of large-scale vertical motion in the atmosphere. *J. Atmos. Sci.*, Vol.56, pp.1248-1258, 1999
12) Raasch, S. and Harbusch, G.: An analysis of secondary circulations and their effects caused by small-scale surface inhomogeneities using large-eddy simulations. *Bound.-Layer Meteorol.*, Vol.101, pp.31-59, 2001
13) Souza, E.P., Renno, N.O. and Silva Dias, M.A.: Convective circulations induced by surface heterogeneities. *J. Atmos. Sci.*, Vol.57, pp.2915-2922, 2000
14) Kottmeier, C. and Engelbart, D.: Generation and atmospheric heat exchange of coastal polynyas in the Weddell Sea. *Bound.-Layer Meteorol.*, Vol.60, pp.207-234, 1992

(Received October 1, 2001)